Metal Target Discrimination with a Commercial Two Frequency Sensor– Part II: Quantitative Aspects

Claudio Bruschini **Luc van Kempen** **Joris Lochy**

École Polytechnique Fédérale de Lausanne – LAP
EPFL-IC-LAP, CH–1015 Lausanne, Switzerland
Claudio.Bruschini@epfl.ch

Vrije Universiteit Brussel – ETRO-IRIS
Pleinlaan 2, B-1050 Brussels, Belgium
lmkempen@etro.vub.ac.be, jlochy@vub.ac.be

Abstract

We have analysed an extensive amount of metal detector raw data using a commercially available differential CW system, the Förster Minex 2FD. Qualitative aspects of the phase response behaviour (signal trajectories in the complex plane) have been detailed in a companion paper [1], showing that a "qualitative" target classification is possible, at least for situations with high Signal to Noise (S/N) ratios. In this article we extend the previous results providing a quantitative analysis.

We define a number of features and propose ways to calculate them in practice from the experimental data sets available. The resulting feature distributions are then analysed and object classification opportunities discussed. Conclusions are then drawn on the possibility of a coarse object classification based on the *object size* and permeability, and on the possibility of discriminating large objects and mines.

1. Introduction

In this article we extend previous results [1] providing a quantitative analysis, which will be partly "phenomenology driven", being based on the actual experimental results of the test samples (debris, mines and their components in particular).

We have opted for a pattern recognition approach in order to estimate the target parameters from measurements. This has arisen in a natural way from the analysis of the response curves in the complex plane, their simplification by extracting a corresponding set of features, and the addition of supplementary features. It is also motivated by the large number of possible clutter shapes and by the number of clutter items usually overwhelming the number of mines.

We briefly recall that frequency domain data has been acquired with a Förster Minex 2FD, a commercially available differential two-frequency continuous wave metal detector (MD) operating at 2.4 kHz (f_1) and 19.2 kHz (f_2) [2]. Linear and parallel scans have been carried out with a high density of points in the scan direction, placing the detector on a Cartesian gantry. First results have been detailed in [2].

The metal detector signals [2]-[3] we are looking at correspond to the real ($f_1 0°$, $f_2 0°$) and imaginary parts ($f_1 90°$, $f_2 90°$) (in the complex plane) of the analog signals $V_1^{(s)}$ and $V_2^{(s)}$ induced at f_1 and f_2 in the receiver. The induced voltages are in fact scaled [2]-[3] to effectively remove their linear dependency on the operating frequency ω, which allows us to compare their ratios and trends with those of a target's theoretical response function.

2. Metal Detector Data Preprocessing

After a preprocessing step, which includes in particular lowpass filtering of the metal detector raw data, Regions of Interest (**RoI**) are defined at each frequency to isolate the part of the data of interest, which is then analyzed in more detail, thereby easing the phase angle peak finding task.

The *imaginary* parts of the signal are in fact usually more affected by the background than the real parts. Some form of filtering would therefore often be beneficial and accordingly a number of tests have been carried out. In the case of the target responses we looked at, their spectral position did however represent a problem, as the low frequency signal components and the background fluctuations did often fall into the same spectral region [3].

Finding a filtering scheme which is valid in most circumstances, i.e. that can guarantee a sufficient level of robustness, turned out therefore to be quite difficult. We have thus chosen to present results considering signals over the chosen RoI without additional filtering, possibly having subtracted the corresponding background files.

3. Feature Definition and Extraction

We will define in the following a number of *features*, i.e. characteristic quantities, and propose ways to calculate them in practice from the experimental data sets available. The features will either be directly derived from the data (e.g. the phase angle response), or from combinations of the data (differential quantities or ratios). Where possible the physics of the problem has been taken into account, for example in the definition of the differential quantities.

Ideal features have a high resolution capability, that is, they are capable of well separating objects belonging to different classes. It will however be sometimes necessary, in particular in presence of background fluctuations, to trade resolution power for applicability and rely on less discriminating features.

3.1. Phase Response

In order to associate one or more phase angles to the signal at f_1 and f_2 we have chosen to look at the **peaks** in the corresponding *phase angle distribution*, using an algorithm detailed in [3].

Examples of the input signals in the complex plane as well as the corresponding phase angle distributions and the resulting selected peaks are shown in the first row of Figure 1. Note that the phase angle values depend on the correct choice of the reference (origin of coordinate system) and that a different number of peaks can be returned at f_1 and f_2. Also, peak selection is usually eased by a correct choice of the RoI (§2).

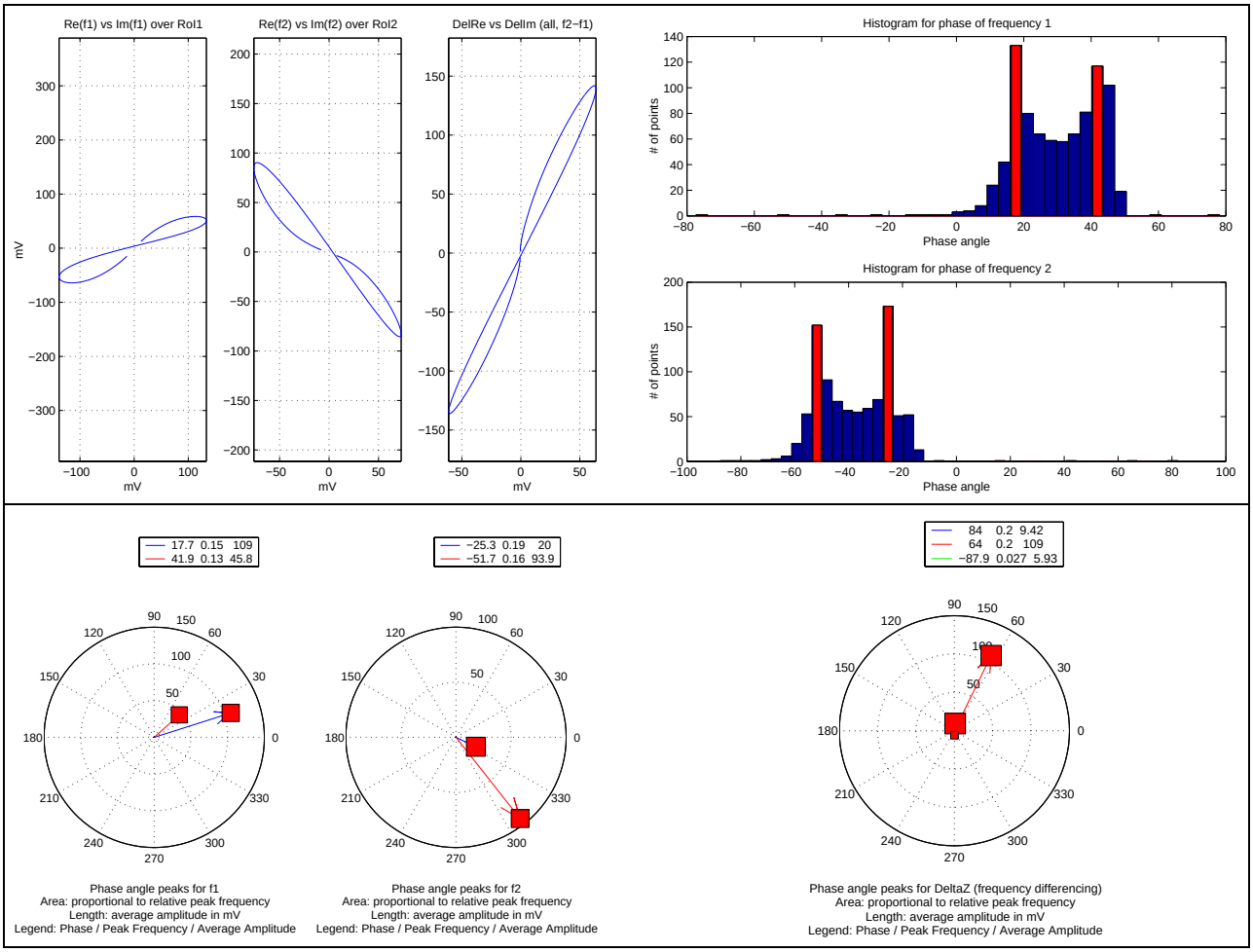

Figure 1: Phase response calculation and phase angle peak representation for a **`PMR-2A`** (stake mine, example of large cylindrical ferromagnetic object) placed vertically. *First row*: complex plane plots (see [1]) and corresponding phase histograms. *Second row*: "combined interface" at f_1 and f_2 (left) and for DeltaZ (right).

3.1.1. Average Amplitude Definition

For each of the selected peaks an **average amplitude** is then calculated by adding the amplitudes of all points having a phase value falling in the same histogram bin as the one of the chosen peak. This reduces noise influence and partially enhances the phase peaks containing data points close to the amplitude maxima, which are usually associated with positions close to the target's centre (where the primary magnetic field is mainly vertical).

3.1.2. Combined Interface

The second row of Figure 1 illustrates a "*combined interface*" in which all information at a given frequency is represented in one polar plot: the *average amplitude* in mV is represented as radial distance (arrow length) whereas each rectangle's area corresponds to the *relative peak height*. These plots do basically represent a simplified version of the complex plane trajectories already detailed in [1], whose main characteristics they do well reproduce.

We note that complex scenarios arise for ferromagnetic and/or composite objects, which are definitely of interest in our application.

3.2. Absolute Amplitude Ratio

Additional features can be extracted from the signal, in particular the ratio of the absolute values ("*Amplitude Ratio*") of the signals induced in the receiver. We have decided to calculate it in two ways, namely 1) as the ratio of the means of the absolute values at f_1 and f_2 (AR1), as well as 2) directly in the complex plane (AR2), whereby we first calculate at each frequency the sum of the distances of the two farthest points, and then take their ratio. The two values usually coincide within 5-10%.

We also define an *average Amplitude Ratio AR* as:

$$AR = \frac{AR1 + AR2}{2} \qquad (1)$$

3.3. Real Part Ratio

As we have seen experimentally, the real component of the received signal is quite unaffected by the background in our experimental conditions and in general for non-conductive soils. It is therefore tempting to use the ratio of the real components at f_1 and f_2 (*ReRatio*) as additional feature. We have decided to calculate it as the ratio of their peak to peak value at the two frequencies:

$$ReRatio = \frac{max(Re(f_1)) - min(Re(f_1))}{max(Re(f_2)) - min(Re(f_2))} \qquad (2)$$

3.4. Other Possible Features

It is possible to define a number of other features, such as the ***L/R*** ratio for a simple circuit model, or a simple differential signal *DeltaZ,* insensitive to fluctuations in the imaginary components. For a detailed analysis see [3].

3.5. Modelling Results for AR and ReRatio

Modelling results for *AR* and *ReRatio** in the case of a sphere and an infinite cylinder transverse to a uniform magnetic field are shown in Figure 2, for *freqRatio*=f_2/f_1=8 typical of the Förster Minex and different permeability values. The target's response parameter α is in both cases equal to $\sigma\mu\omega r^2$, the product of the target's conductivity σ, permeability μ and radius *r* squared, times the operating frequency ω.

ReRatio grows monotonically, reaching about 2.8 at the inductive limit in both cases. *AR* for permeable objects features one peak above and one below the *AR*=1 line, at about the same height for the permeability values shown. The value of the highest peak is of about 1.9 for the sphere and 1.6 for the cylinder, of the lowest about 0.7 for the sphere and 0.65 for the cylinder. It is in particular impossible to have a situation, for the transverse cylinder, in which both *AR* and *ReRatio* are larger than 1. This is however possible for a permeable sphere over a restricted range of induction parameter values.

The behaviour at larger permeability values is similar to the one shown. It is however different for *low permeability values*, as could be the case for some stainless steels.

3.6. Comparison with Model Expectations

Results from some of the test objects, in particular cylinders, have been compared with what is expected from theoretical models for a sphere and an infinite transversal cylinder. In general agreement is quite good, with obvious exceptions for ferromagnetic cylinders when aligned along the primary magnetic field (demagnetization effects) [3].

---

* Labelled *ImRatio* in the plots, as they show the behaviour of an object's response function [2]-[3] rather than of the measured data. The response function has indeed to be multiplied by a term containing a factor $i\omega$, equivalent to a 90° counter-clockwise rotation in the complex plain, to obtain the induced voltage.

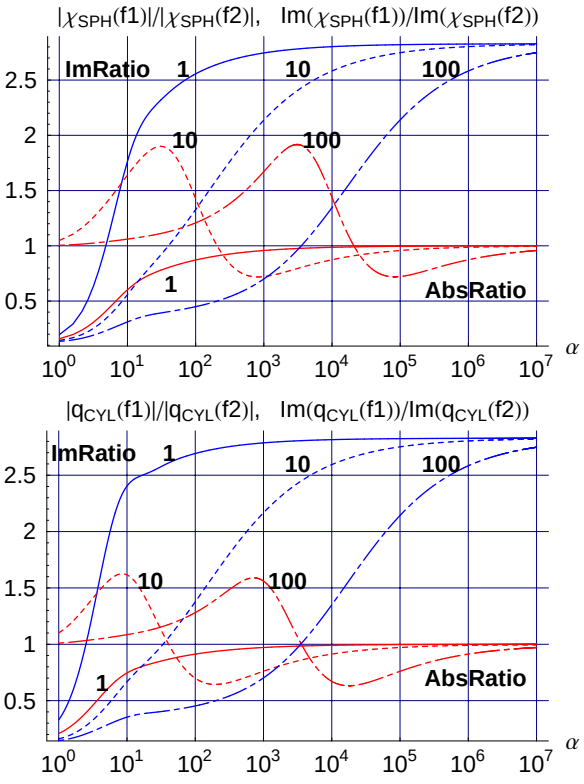

Figure 2: Ratios of the imaginary part (*ImRatio*) and absolute value (*AbsRatio*) of a target's response function at $f_2=8f_1$ (Förster Minex parameters) for a non-ferromagnetic ($\mu_r=1$, continuous) and ferromagnetic objects ($\mu_r=10$: dashed, $\mu_r=100$: dot-dashed). *Top*: sphere (χ_{SPH}), *Bottom*: transverse infinite cylinder (q_{CYL}). In both cases: $\alpha=\sigma\mu\omega r^2$.

4. Classification Opportunities

In the following we will analyse the distribution of the previously defined features and discuss the resulting object classification opportunities, that is the possibility of attributing a measurement to a specific object class.

The actual values of some features are obviously dependent on the parameters used for their extraction; they are also specific of the Förster Minex operating parameters. The results should nevertheless still be of general interest and it should not be too difficult to extrapolate them to other operating conditions.

"Small" vs. "Large" Objects

The features we are looking at are basically derived from the target's response function and as such do depend on its *response parameter* (or induction number) and magnetic permeability, as well as on its orientation (influence of the demagnetization factor) for most ferromagnetic objects [1],[3]. A target's *response parameter* is usually a product of permeability, conductivity and the square of an average linear dimension of the target, thereby putting a particular weight on its size.

In the following we will therefore often refer to an *object size* using terms such as "*small*" and "*large*"; *strictly speaking we are however discriminating on the full response parameter rather than on its physical size only.*

4.1. Phase Angle Peaks and Amplitude Ratio

We analyse the distribution of the phase angle peaks and of the (average) *Amplitude Ratio AR* using 3D scatter plots, each phase angle peak φ_j being represented as a point in 3D space with cylindrical coordinates $\theta=\varphi_j$, $\rho=1$ and $z=AR$. In addition we plot for each point its projection on the x-y plane and connect it with a line to the origin (actually on a plane at $z = -0.5$ for graphical reasons), to make it easier to determine each point's phase angle.

The use of such 3D plots, although not strictly necessary to represent the distribution of the chosen features, does help in comparing the results with the original complex plane plots. (Bidimensional plots might well be employed in the future.) Examples are shown in Figure 3, plotting only the highest average amplitude peaks. Points at f_1 are shown with dots, at f_2 with squares. Note that the scale along *x* is 1/2 of the scale along *y*. *The resulting distributions of the phase angle peaks only,* i.e. the projections on the x-y plane, *confirm in a quantitative way the qualitative results detailed in* [1].

In addition the complete distributions (i.e. considering *AR* as well) detail how different object categories, in particular debris, can form *clusters* in the chosen 3D space. Examples are provided in Figure 3 for some of the debris collected from a simulated minefield during field tests of a GPR prototype in Cambodia [1],[3]: non-ferromagnetic foils (`deb20-26`) are shown in the top half (very low *AR*), all collected ferromagnetic debris in the bottom half ($1<AR<2.2$ with a couple of exceptions). Note in particular the trend, in this last case, of decreasing phase angle with increasing *Amplitude Ratio*. The corresponding *AR* distribution is detailed in Figure 4 ($AR>1$ for all ferromagnetic objects, $AR<1$ for the two non-ferromagnetic ones).

Amplitude Ratio Distribution

The *Amplitude Ratio* distribution of the **debris** collected

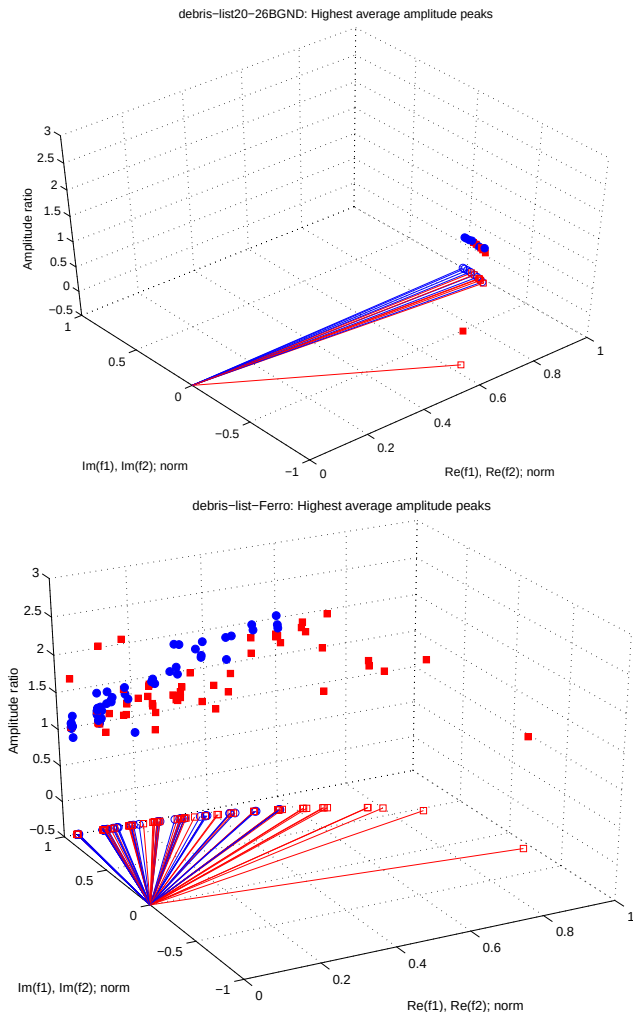

Figure 3: Phase angle peaks (highest average amplitude only) vs. average *Amplitude Ratio AR* for some representative debris: *Top*: non-ferromagnetic foils (**deb20-26**), *Bottom*: **all ferromag. debris.** Dots: values at f_1, squares: values at f_2.

in Cambodia can be deduced from Figure 4, where each small square corresponds to a debris object in a given setup. The debris in the top left (**deb01-16**) is mostly ferromagnetic (nails, plates, a bottle cap, ...), the one in the top right (**deb70-82**) miscellaneous (foils, nails, a bullet, shell fragments, ...). Where a symmetry suggested a possible orientation-dependent response each object has been measured parallel (*PAR*) and perpendicular (*PER*) to the metal detector scanning axis. All measurements of the **non-ferromagnetic debris** are collected in the bottom left part of Figure 4, the ones of the **ferromagnetic debris** in the bottom right part.

The *Amplitude Ratio* distribution of some representative **targets** can be deduced from Figure 5, where each small square corresponds to an object in a given setup. *Top*: mines with a small metallic content [1],[3]: a complete minimum-metal AP mine (**mich**) and its components, i.e. a detonator (real: **midereal**, replica: **mide**) and a steel striker pin (**mist**), and a Vietnamese MD-82B AP mine (**miviet**). *Bottom*: mines with larger metallic content: a PMN (**pmnVUB**), fragmentation metallic mines (bounding: **PROM**, stake: **PMR**-2A), and a composite object, a 20 mm projectile (**bull**). Some of the targets have been placed vertically (*VER*) as well. The distribution of several classes of targets of interest is superposed on to Figure 4.

The main characteristics of the *Amplitude Ratio distribution* are:

- ***AR*>1** is typical of **ferromagnetic** objects, where ***AR*~1-1.2** for *flat* and ***AR*>1.5** for *elongated* targets when there is a significant component of the magnetic field along the symmetry axis (e.g. *PAR*, *VER* orientations).

  In general: *AR*(*PAR*, *VER* orientations) > *AR*(*PER* orientation) for a given elongated object, and similarly for ReRatio.
- ***AR*<0.2-0.3** is typical of **small non-ferromagnetic** objects (e.g. foils), and **0.7<*AR*<1** is typical of **large** non-ferromagnetic objects (e.g. **deb100-104**, Figure 4) or large ferromagnetic ones (e.g. **PROM** mine, Figure 5).

These results are in general in good agreement with model expectations. As discussed in §3.5 a maximum value of about 1.9 is foreseen for a sphere and of 1.6 for a transversal (infinite) cylinder using the Förster Minex operating parameters (see Figure 2).

4.2. Amplitude Ratio vs. Real Part Ratio

Examples of the average *Amplitude Ratio AR* vs. *ReRatio* distribution are shown in Figure 4 and Figure 5. It is evident that the two features are correlated: the higher *AR*, the higher *ReRatio*, with some exception for very large ferromagnetic objects. This corresponds to a trend from small objects in the lower left corner (all *non-ferromagnetic* debris plot of Figure 4) to large ones in the upper right corner. This implies that for non-ferromagnetic objects one can extrapolate to a certain extent the size from the *AR* vs. *ReRatio* plot, which is generally not true for ferromagnetic objects without some a priori knowledge of target type and/or orientation.

In the case of the *debris* most non-ferromagnetic objects are *below* the *AR=ReRatio* line (dashed in Figure 4), as correctly predicted by the sphere and cylinder model

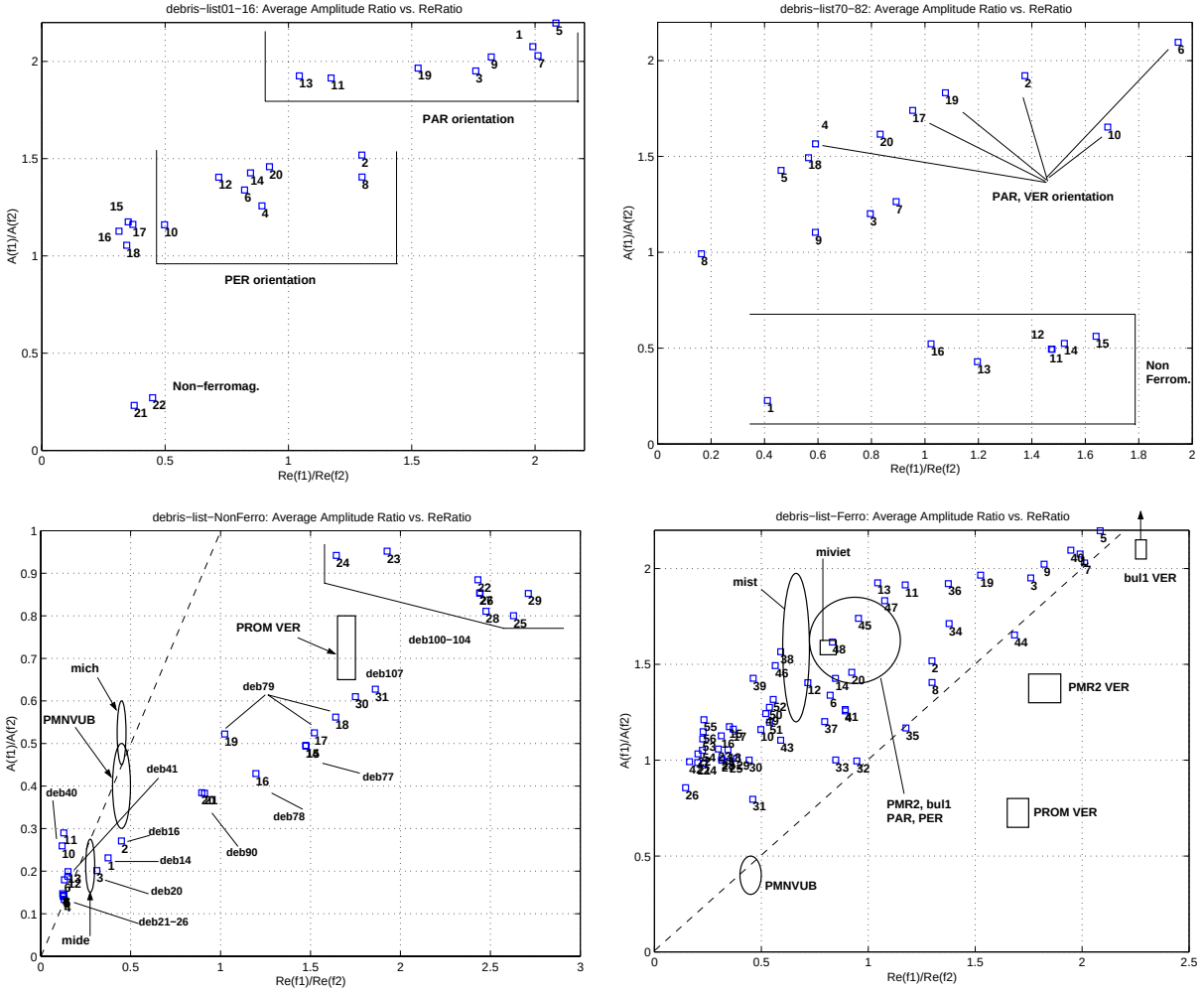

Figure 4: Average *Amplitude Ratio AR* vs. *ReRatio* for *debris* and some representative *targets*. *Top left*: mostly ferromagnetic debris (**`deb01-14&16`**, see text), *Top right*: miscellaneous debris (**`deb70-82`**, see text), *Bottom left*: **`all non-ferromagnetic debris`**, *Bottom right*: **`all ferromagnetic debris`**.

(§3.5), whereas all ferromagnetic *debris* is *above* it. The models also foresee a maximum *ReRatio* of about 2.8, which is experimentally well verified.

It is interesting to note that some very large ferromagnetic objects could be distinguished on the basis of their (*AR,ReRatio*) values alone, for example a vertical **`PMR-2A`** or **`bul1`**. *In general however only a partial target discrimination seems possible using the (AR,ReRatio) values alone*, as evident from the bottom plots in Figure 4. The residual ambiguity can be resolved in a number of cases using the phase response information.

ReRatio Distribution

The *ReRatio* distribution by itself presents the following characteristics:

- ***ReRatio*<0.2-0.3** is typical of small non-ferromagnetic objects such as foils or wire strands. This is mostly true also for similar ferromagnetic objects, whereas ***ReRatio*>2.0-2.5** is typical of large non-ferromagnetic objects.
- **In general: *ReRatio*(*PAR*, *VER* orientations) > *ReRatio*(*PER* orientation) for a given elongated ferromagnetic object**, similarly to the *AR* behaviour.

ReRatio works therefore well to discriminate very large or very small non-ferromagnetic objects. It does however not seem to be sufficiently robust, used by itself, for ferromagnetic objects. Some targets could be discriminated on the basis of their *ReRatio* alone, such as the small mine components, however likely at the price of a high false alarm rate.

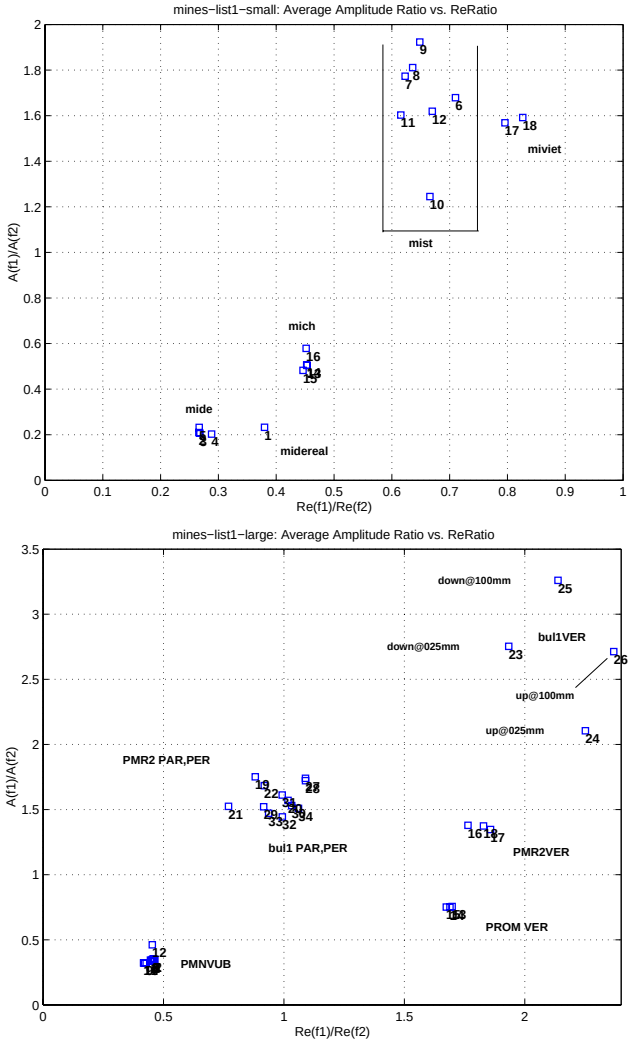

Figure 5: Average *Amplitude Ratio AR* vs. *ReRatio*. *Top*: **`low metal`** content mines and their components, *Bottom*: **`PMN`** AP mine and **`large metallic mines/UXO.`**

5. Conclusions

Whereas the companion article [1] focused more on the qualitative aspects of a metal detector's phase response behaviour to targets of interest in humanitarian demining applications, in this article we have defined a number of features, processed the available data and analysed the resulting distributions.

5.1. Overall Considerations

The peak finding algorithm in particular seems to be working well; this allows to reduce the detailed curves in the complex plane to a coarser information, basically the phase angle peaks and their average amplitudes. Multiple peaks are usually characteristic of composite or ferromagnetic objects, or for low S/N scenarios. One large ferromagnetic peak is usually strongly indicative of a ferromagnetic component.

Most of the information seems to be contained in the phase response. There are however cases in which the use of the *Amplitude Ratio AR*, and of the *ReRatio*, provides additional information, in particular helping in resolving ambiguities. In general only a partial target discrimination seems possible using the (*AR,ReRatio*) values alone.

The theoretical models' predictions on the behaviour of *AR* and *ReRatio* are confirmed by the experimental data. Important demagnetization effects are apparent for elongated ferromagnetic objects, for which *AR*(*PAR*, *VER* orientations) > *AR*(*PER*), and similarly for *ReRatio*.

5.2. Main Conclusions

A) Coarse Object Classification Possibilities

A coarse target classification according to the *object size*, as defined at the beginning of §4, and permeability (ferromagnetic or not), seems indeed to be possible, at least for scenarios with a sufficient S/N ratio.

The decision could be taken by the user himself relying on a **visual interface** of the type discussed in [1] (*complex plane curves*), or using a simplified bidimensional information like the *phase angle peaks*, possibly augmented by an indication of the *Amplitude Ratio* if necessary. A simple alternative could be represented by a plot in the *AR* vs. *ReRatio* plane. An alternative is represented by an **automated system** with a direct output indicating the most likely *object size* and permeability (ferromagnetic or not). This could be combined if necessary with a 2D diagram of the phase response.

Whether these type of approaches are sufficient for actual mine discrimination is discussed at C).

In the low S/N case detection is still possible but classification gets increasingly difficult. Apart from deciding not to attempt classifying a signal with insufficient S/N, when the main features can not be used reliably any more it should still be possible to exploit additional features such as *ReRatio*, $L/R|_{\Delta Weighted}$ and *DeltaZ* albeit with reduced discrimination capabilities [3].

B) Large Metallic Mines/UXO Discrimination

Our initial idea was to discriminate large targets relying on their phase response, for example by imposing a

threshold on the phase. The results for some large metallic objects (**PROM**, **PMR**, **bul1**) confirm that this is possible, at least for the objects we looked at. Composite objects do however deserve a closer look, and it can be necessary to complement the phase response with *AR* to resolve ambiguities, such as in the case of a **PROM** mine.

We initially hoped to extend this discrimination approach also to mines with an average metallic content (e.g. **PMN**, **PMN2**). Judging from the experimental results this might be possible for the **PMN** if the signature from the mine's cover retaining ring is reasonably stable. It looks more difficult for the **PMN2**, which is composed of about 10 pieces of various sizes.

C) Mine Discrimination

Discriminating mines from clutter or even different mines among themselves looks feasible; in the end it depends however on the following factors:

C1) Which and how many types of mines are present (*a priori* knowledge).

If we are for example looking for minimum-metal mines containing a detonator similar to the **mide** previously analysed, we could in principle discard all ferromagnetic objects. Too many different target types are however likely to make a purely visual choice quite difficult.

C2) How much one can rely on stable mine signatures. This influences the tolerance "windows" which will have to be applied around the known targets of interest. We can distinguish two aspects here: *differences at the mine component level*, and *differences in the behaviour of a given type of object*.

The first point includes manufacturing differences as well as the use of different components altogether. Along the same lines [4] discusses differences in the response of a "new" and an "old" PMN mine due to rusting of the cover retaining ring. The second point relates mostly to changes in the response of ferromagnetic or composite objects for different orientations/distances.

Note that the fact of having to look at too many different objects and/or of having to use too large windows will probably affect the selectivity of the procedure and the resulting false alarm rate.

C3) How representative the debris we had available is, and how often multitarget scenarios are encountered.

C4) How many clutter objects have a sufficient S/N ratio to allow discrimination.

Indeed, even provided that one can discriminate mines from clutter, the actual **system effectiveness** will depend on how much the **false alarm rate** can be reduced, i.e. *how many times a clutter item has a sufficient S/N ratio to be identified as such*. In other words, clutter is usually vastly majoritary; therefore, even if we could identify each mine but for example only 10% of the clutter had a sufficient S/N (i.e. in nearly 90% of the cases we would have to issue an "unknown object type" response), the system would probably not be too useful. An object's S/N ratio is influenced in particular by its *depth* and *size*. Additionally the soil type does obviously play a crucial role.

In situations where one can not rely on stable signatures it could still be possible to exclude certain types of clutter; it remains however to be seen how useful this is.

Acknowledgment

The members of the former EPFL/DeTeC team, in particular Frédéric Guerne and Bertrand Gros, built the gantry and data acquisition electronics and thus made data acquisition and collection possible. Many colleagues at VUB-ETRO, in particular Valentin Enescu and Timofei Savelyev, did play an important role in system setup and data acquisition. This work has been partially supported by the Swiss Office for Education and Science (OFES) within the EC IST EUDEM2 project (**www.eudem.info**).

6. References

[1] C. Bruschini, "Metal Target Discrimination with a Commercial Two Frequency Sensor–Part I: Raw Data Analysis in the Complex Plane", these proceedings.

[2] C. Bruschini and H. Sahli, "Phase angle based EMI object discrimination and analysis of data from a commercial differential two frequency system", in *SPIE Proceedings Vol. 4038,* pp. 1404-1419, Orlando, FLA, April 24-28, 2000.

[3] C. Bruschini, "A Multidisciplinary Analysis of Frequency Domain Metal Detectors for Humanitarian Demining", PhD Thesis, Vrije Universiteit Brussel (VUB, Belgium), Faculty of Applied Sciences, Brussels, Belgium, Sept. 2002, 230 pp. Also available from: http://www.eudem.info/

[4] P. Druyts, Y. Yvinec, and L. Merlat, "Signal processing tools for standard metal detectors (Imaging and Signature mode)", in *Proc.* of the *Research on Demining Technologies Joint Workshop*, Joint Research Centre (JRC), Ispra, Italy, 12-14 July 2000.